

# Light Water Reactor Sustainability Program

## Assessment of the Efficiency of HWC on the IASCC Crack Growth Rate for High-Fluence BWR Materials



September 2016

U.S. Department of Energy  
Office of Nuclear Energy

**DISCLAIMER**

This information was prepared as an account of work sponsored by an agency of the U.S. Government. Neither the U.S. Government nor any agency thereof, nor any of their employees, makes any warranty, expressed or implied, or assumes any legal liability or responsibility for the accuracy, completeness, or usefulness, of any information, apparatus, product, or process disclosed, or represents that its use would not infringe privately owned rights. References herein to any specific commercial product, process, or service by trade name, trade mark, manufacturer, or otherwise, does not necessarily constitute or imply its endorsement, recommendation, or favoring by the U.S. Government or any agency thereof. The views and opinions of authors expressed herein do not necessarily state or reflect those of the U.S. Government or any agency thereof.

# **Assessment of the Efficiency of HWC on the IASCC Crack Growth Rate for High-Fluence BWR Materials**

**S. Teysseyre**

**September 2016**

**Prepared for the  
U.S. Department of Energy  
Office of Nuclear Energy**



## **ABSTRACT**

This report describes the experimental study performed to assess the efficiency of hydrogen water chemistry on the propagation rate of cracks generated by irradiation-assisted stress corrosion cracking in high-fluence materials. This report presents the selection of the material and the test procedures followed for this study. The test results obtained with 8.6 dpa specimens are discussed. At this point in the study, it appears that hydrogen water chemistry is still efficient at lower applied stress intensity factor. However, as the stress intensity factor increased, the crack propagation rate increased sharply. The reason for this increase in crack propagation rate is being investigated.



# CONTENTS

ABSTRACT.....	iii
ACRONYMS.....	vii
1. INTRODUCTION.....	9
2. EXPERIMENTAL PROCEDURE.....	9
2.1 Material.....	9
2.2 Specimen.....	10
2.3 Irradiation-Assisted Stress Corrosion Cracking Crack Growth Rate Test Procedure.....	10
3. IRRADIATED STRESS CORROSION CRACKING TEST RESULTS AND DISCUSSION.....	13
4. DEFORMATION MICROSTRUCTURE CHARACTERIZATION PROCEDURE.....	21
5. CONCLUSION.....	24
6. REFERENCES.....	24

# FIGURES

Figure 1. Schematic of a 0.5 T-CT specimen ( $B = 5.6$ mm).....	10
Figure 2. Schematic of the IASCC CGR test facility used for this work at the NFD facility.....	12
Figure 3. Picture of the autoclaves located in the hot cell NFD facility. ....	12
Figure 4. Crack length and $K$ applied during the course of the experiment. ....	14
Figure 5. Crack length and corrosion potential versus time during the course of the experiment. ....	15
Figure 6. Outlet conductivity and temperature versus time during the course of the experiment. ....	16
Figure 7. Fracture surface of the CT specimen. ....	17
Figure 8. Comparison between the CGR generated during this study and reported data (JNES 2009).....	18
Figure 9. Comparison between plastic collapse criteria and our experimental results. ....	19
Figure 10. Comparison between $K$ -validity criteria based on $B$ and our experimental results.....	20
Figure 11. Comparison between $K$ -validity criteria based on $(W-a)$ and experimental results. ....	20

Figure 12. Location of the depth at which the various K-validity criteria were breached on the fracture surface. ....	21
Figure 13. Schematic showing where the test specimen was sampled for analysis of the deformation microstructure. ....	22
Figure 14. Lift out the transmission electron microscopy specimens for deformation microstructure characterization. ....	22
Figure 15. Transmission electron microscopy specimen removed near the IASCC crack in an area corresponding to a crack growing in respect to the K-validity criteria.....	23
Figure 16. Transmission electron microscopy specimen removed near the IASCC crack in an area corresponding to all K-validity criteria that were breached.....	24

## TABLES

Table 1. Chemical compositions of base metals (mass %). ....	9
Table 2. Summary of tensile tests (304 SS, 288°C in air, strain rate $3 \times 10^{-4} \text{ s}^{-1}$ ).....	10
Table 3. Loading and chemical conditions applied during the experiment. ....	13
Table 4. Measured anion concentration during the experiment. ....	13
Table 5. CGR obtained for the various test conditions applied. ....	17

## ACRONYMS

BWR	boiling water reactor
CGR	crack growth rate
CT	compact tension
ECP	electrochemical corrosion potential
HWC	hydrogen water chemistry
IASCC	irradiation-assisted stress corrosion cracking
NFD	Nippon Nuclear Fuel Development Co, Ltd
NWC	normal water chemistry



# Assessment of the Efficiency of HWC on the IASCC Crack Growth Rate for High-Fluence BWR Materials

## 1. INTRODUCTION

Hydrogen water chemistry (HWC) has been well established as an efficient mitigation technique for stress corrosion cracking. With unirradiated materials, the crack growth rate (CGR) measured in HWC can be 5 to 50 times lower than those obtained in normal water chemistry (NWC) (Andresen et al. 2002, Andresen and Morra 2008). In the NRC-NUREG-0313 report (Hazelton and Koo 1988), the HWC mitigation efficiency is credited with a factor of 3.

When looking into the behavior of stainless steels irradiated above  $3 \times 10^{21}$  n/cm<sup>2</sup> (about 4.5 dpa for stainless steels), data suggest that mitigating CGR by using HWC may not be efficient as dose increases. Jensen et al. (2003) tested a control blade material that was in operation for about 23 years. The material accumulated about 12 dpa and was tested to a K up to 18 MPa√m. They observed a high CGR in HWC and concluded that, under such testing conditions, HWC did not mitigate irradiation-assisted stress corrosion cracking (IASCC). However, while testing a 304L core shroud material irradiated in the BOR60 fast reactor at 5.5 and 10.2 dpa, Jensen et al. (2003) observed lower CGR when testing at low corrosion potential; however, they did not see any K dependency between K = 11 MPa√m and K = 18 MPa√m (Jensen et al. 2009). Takamura et al. (2009) measured CGR for 316L and 304L tested in a boiling water reactor (BWR) environment. They looked at the effect of electrochemical corrosion potential (ECP) as fluence increases on CGR. Their findings suggest that the effect of ECP on CGR becomes weak when applied K is greater than 20 MPa√m.

To ensure safe operation of our nuclear reactors, it is important to determine the conditions for a decrease, or loss, of efficiency of HWC to mitigate CGR and to understand the mechanism involved. This report presents the experimental procedure and initial results of that investigation.

## 2. EXPERIMENTAL PROCEDURE

### 2.1 Material

The material tested came from a Japanese national project. The specimens were irradiated in the Japanese Material Test Reactor in BWR conditions (e.g., temperature of 288°C [262 to 302°C] and conductivity below 0.1 μS/cm (Takamura et al. 2009, Nakamura et al. 2007) at a flux of  $1 \times 10^{18}$  n/m<sup>2</sup>-s) from 2001 through 2006. The material tested has been irradiated to 8.6 dpa.

The specimen was machined from an unirradiated 38-mm thick plate of Type 304 stainless steel. The chemical composition of the base metal is shown in Table 1 (JAPEIC 2003). A heat treatment (i.e., 1030°C × 30 minutes followed by water quench) was applied to simulate the fusion line of the weld heat affected zone (HAZ). The intent is to be representative of welding conditions consistent with those from typical BWR core components.

Material tensile properties have been determined by the Japanese program; results from tensile tests conducted in air at 288°C are summarized in Table 2 (JNES 2007). Tested specimens R433 and R435 have identical neutron fluence as the specimen used for our CGR test.

Table 1. Chemical compositions of base metals (mass %).

Alloy	C	Si	Mn	P	S	Ni	Cr	Mo	Co
304	0.005	0.65	1.20	0.024	0.004	8.93	18.58	—	0.04

Table 2. Summary of tensile tests (304 SS, 288°C in air, strain rate  $3 \times 10^{-4} \text{ s}^{-1}$ )

Specimen ID	Dose (dpa)	0.2% Proof Stress (Mpa)	Tensile Stress (Mpa)	Uniform Elongation (%)	Total Elongation (%)
R433	11.3	786	787	0.3	8.8
R435	10.2	793	795	0.3	8.9

## 2.2 Specimen

The 0.5 T-compact tension (CT) specimens, cut in the T-S orientation, were machined from the base metal plate. For this irradiation program, three kinds of specimen thickness were prepared in order to prevent the rise of specimen temperature caused by gamma heating and keep the specimen temperature in the range of 262 to 302°C during irradiation. The tested specimen was 5.6 mm thick. The specimen has side grooves with a 5% depth of the thickness on each side surface. Prior to irradiation in high-temperature water, a fatigue pre-crack was introduced to the specimens through cyclic loading at room temperature in air to a depth of 1.5 mm ( $a/W = 0.45$ ). The maximum stress intensity factor (i.e.,  $K_{max}$ ) values at the end of the fatigue pre-cracks were adjusted to  $12 \text{ MPa}\sqrt{\text{m}}$ . Figure 1 shows the schematic of the CT specimen. Specimen A128 (R403) was used for the CGR test.

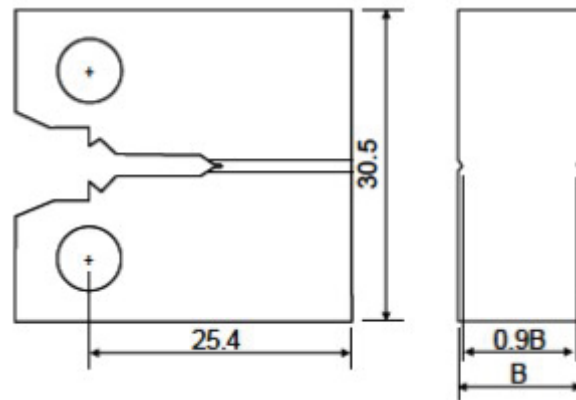


Figure 1. Schematic of a 0.5 T-CT specimen ( $B = 5.6 \text{ mm}$ ).

## 2.3 Irradiation-Assisted Stress Corrosion Cracking Crack Growth Rate Test Procedure

A CGR test was conducted under applied constant load in simulated BWR water at 288°C. This test has been performed in Nippon Nuclear Fuel Development Co, Ltd (NFD) facilities. The facilities are schematically illustrated in Figures 2 and 3. As indicated in Figure 2, the autoclaves where the specimens are installed and loaded are located in the hot cell, while the equipment related to water chemistry control and operation of the water loop are placed outside the hot cell. This system can perform testing in simulated BWR and pressurized water reactor (PWR) environments. Each autoclave can accommodate two 0.5 T-CTs or one 1 T-CT. The dissolved oxygen concentration is measured continuously at the inlet and the outlet. Conductivity is measured continuously at the outlet and measured periodically at the inlet. Progression of the crack is monitored using the reverse direct current potential drop method. The electrochemical corrosion potential (ECP) of the specimen was monitored using an internal or external Ag/AgCl reference electrode.

Prior to the constant load CGR test, “gentle” cycling (i.e.,  $R 0.7$ , 0.001 to 0.0001 Hz) was introduced under NWC conditions ( $\geq 130 \text{ mVSHE}$ ) at 288°C until crack growth exceeds the plastic zone associated with fatigue pre-cracking. The CGR data under NWC conditions were acquired first and ECP was

changed to HWC condition ( $\leq -200$  mVSHE) to examine the effect of ECP on CGR. After CGR at the HWC condition was measured, the environment was changed back to the NWC condition. After having obtained a stable crack growth in NWC, the environment was changed again to HWC condition. The anion (i.e.,  $\text{SO}_4^{2-}$ ,  $\text{Cl}^-$ ,  $\text{NO}_3^-$ ) concentration in the test water was measured periodically using an ion chromatograph and sampling the inlet and the outlet water. The concentration was maintained to less than 5 ppb.

It was decided to apply an initial stress intensity factor  $K$  of  $13 \text{ MPa}\sqrt{\text{m}}$  after considering the suggested various  $K$ -validity criteria. This determination was based on the material's tensile properties:

- Tensile properties for 10 dpa 304 stainless steel  
 $\sigma_y$  at 288 C : 790 MPa
- Tensile properties for unirradiated 304 stainless steel  
 $\sigma_y$  at 288 C : 156 MPa.

The following  $K$ -validity criteria were considered:

- According to Andresen (-2003) :

$$B_{eff}, W - a \geq 2.5 \left( \frac{K}{\sigma_{eff}} \right)^2$$

With  $\sigma_{eff} = (\sigma_{y_{unirr}} + (\sigma_{y_{irr}} + \sigma_{y_{unirr}})/3)$

Which gives:  $K_I < 18.0 \text{ MPa}\sqrt{\text{m}}$ .

- According to Jensen et al. (2003) :

$$B_{eff}, W - a \geq 2.5 \left( \frac{K}{\sigma_{eff}} \right)^2$$

With  $\sigma_{eff} = (\sigma_{y_{irr}} + \sigma_{y_{unirr}})/3)$

Which gives:  $K_I < 15.5 \text{ MPa}\sqrt{\text{m}}$

- According to Kumar (1981, 1984):

$P_c: 1.455 \eta B \sigma (W)$

$$\text{Where } \eta = \left\{ \left( \frac{2a}{W-a} \right)^2 + \left( \frac{4a}{W-2} \right) + 2 \right\}^{0.5} - \left( \frac{2a}{W-2} \right)$$

Where  $W$  is the specimen width,  $B$  is its thickness,  $a$  the crack length,  $\sigma$  the flow stress,  $\sigma_y$  the yield stress,  $\sigma_{y_{unirr}}$  the yield stress of the unirradiated material, and  $\sigma_{y_{irr}}$  the yield stress of the irradiated material.

However, the system does not control  $K$ ; it only controls the load. The test was performed at constant load, with the  $K$  being dependent on the crack advance. For this test, load shedding was not applied to attempt to maintain a constant  $K$ .

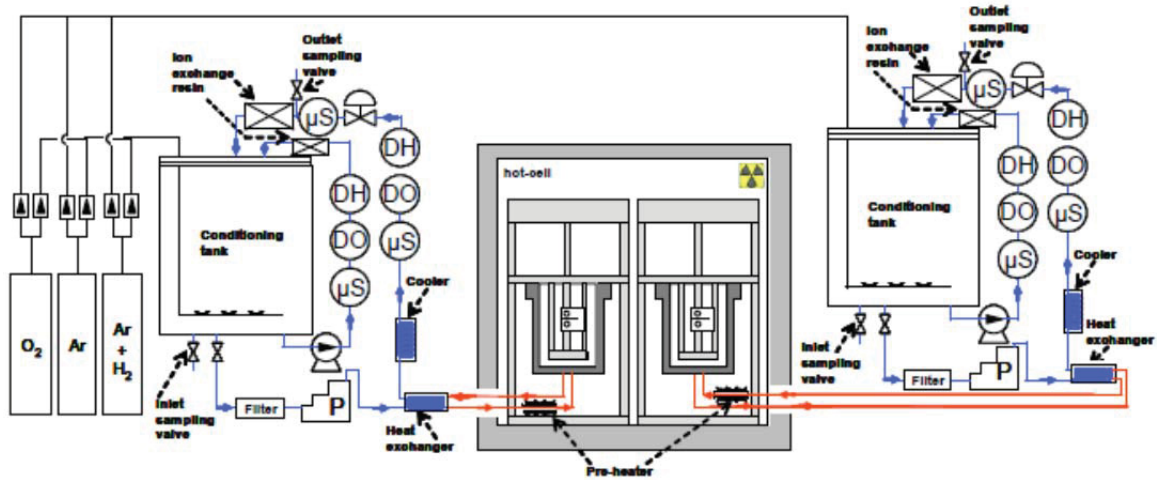


Figure 2. Schematic of the IASCC CGR test facility used for this work at the NFD facility.

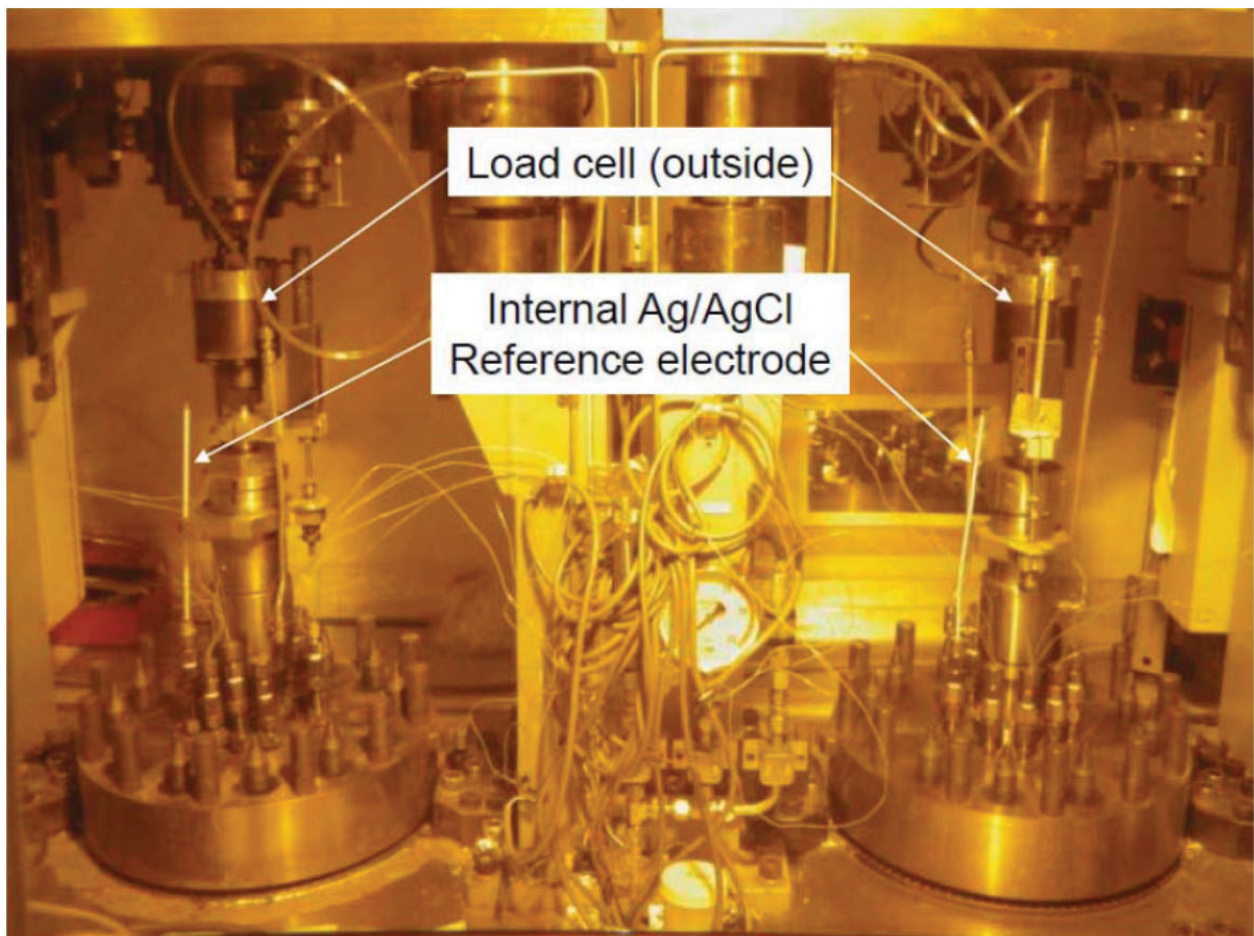


Figure 3. Picture of the autoclaves located in the hot cell NFD facility.

### 3. IRRADIATED STRESS CORROSION CRACKING TEST RESULTS AND DISCUSSION

The test conditions during the test run are summarized in Table 3. Measured anion concentrations ( $\text{SO}_4^{2-}$ ,  $\text{Cl}^-$ ,  $\text{NO}_3^-$ ) during the test are summarized in Table 4. The crack growth behavior and environment history during the test are summarized in Figures 4 through 6. The obtained CGR data are shown in Table 5. The CGRs shown in this table were initially estimated by direct current potential drop measurement and were corrected based on the post-test analysis of the fracture surface. Observed fracture surface photographs are shown in Figure 7.

Table 3. Loading and chemical conditions applied during the experiment.

Test Stages		Dissolved Oxygen (ppm)	ECP (mVshe)	Frequency (Hz)	Loading Ratio (R)
Stage 0	Stage 0-1	32	>130	0.001	0.7
	Stage 0-2	32	>130	0.0001	0.7
Stage 1		32	>130	Constant load	
Stage 2		0.01	<-200	Constant load	
Stage 3		32	>130	Constant load	
Stage 4		0.01	<-200	Constant load	

Table 4. Measured anion concentration during the experiment.

	Before the Experiment		During the Experiment						After the Experiment	
			Month 1		Month 2		Month 3			
	Inlet	Outlet	Inlet	Outlet	Inlet	Outlet	Inlet	Outlet	Inlet	Outlet
$\text{SO}_4^{2-}$ (ppb)	<2	<2	<2	<2	<2	<2	<2	<2	<2	<2
$\text{Cl}^-$ (ppb)	<2	<2	<2	<2	<2	3.3	<2	2.2	<2	2.2
$\text{NO}_3^-$ (ppb)	<2	<2	<2	<2	<2	<2	<2	<2	<2	<2

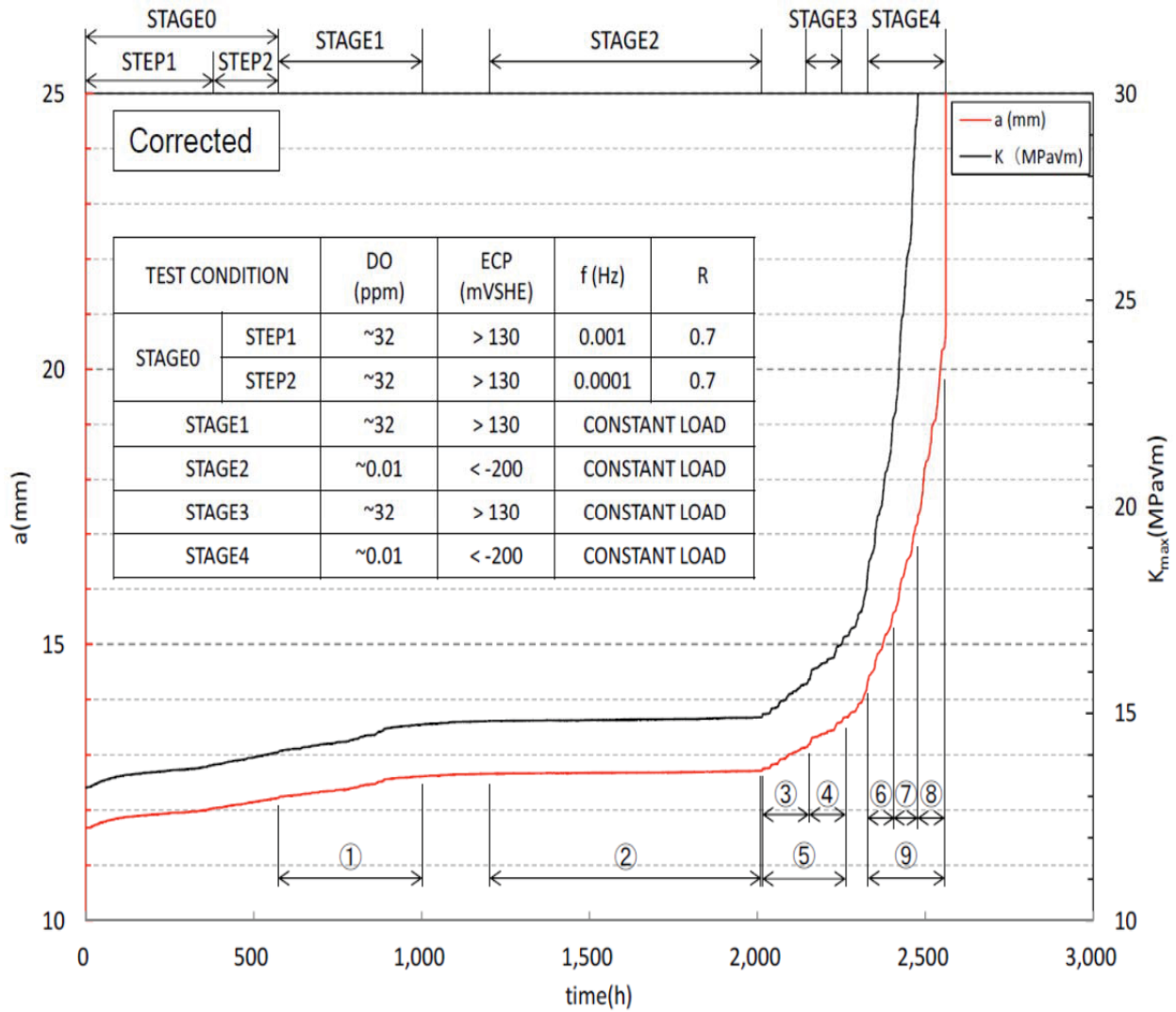


Figure 4. Crack length and K applied during the course of the experiment.

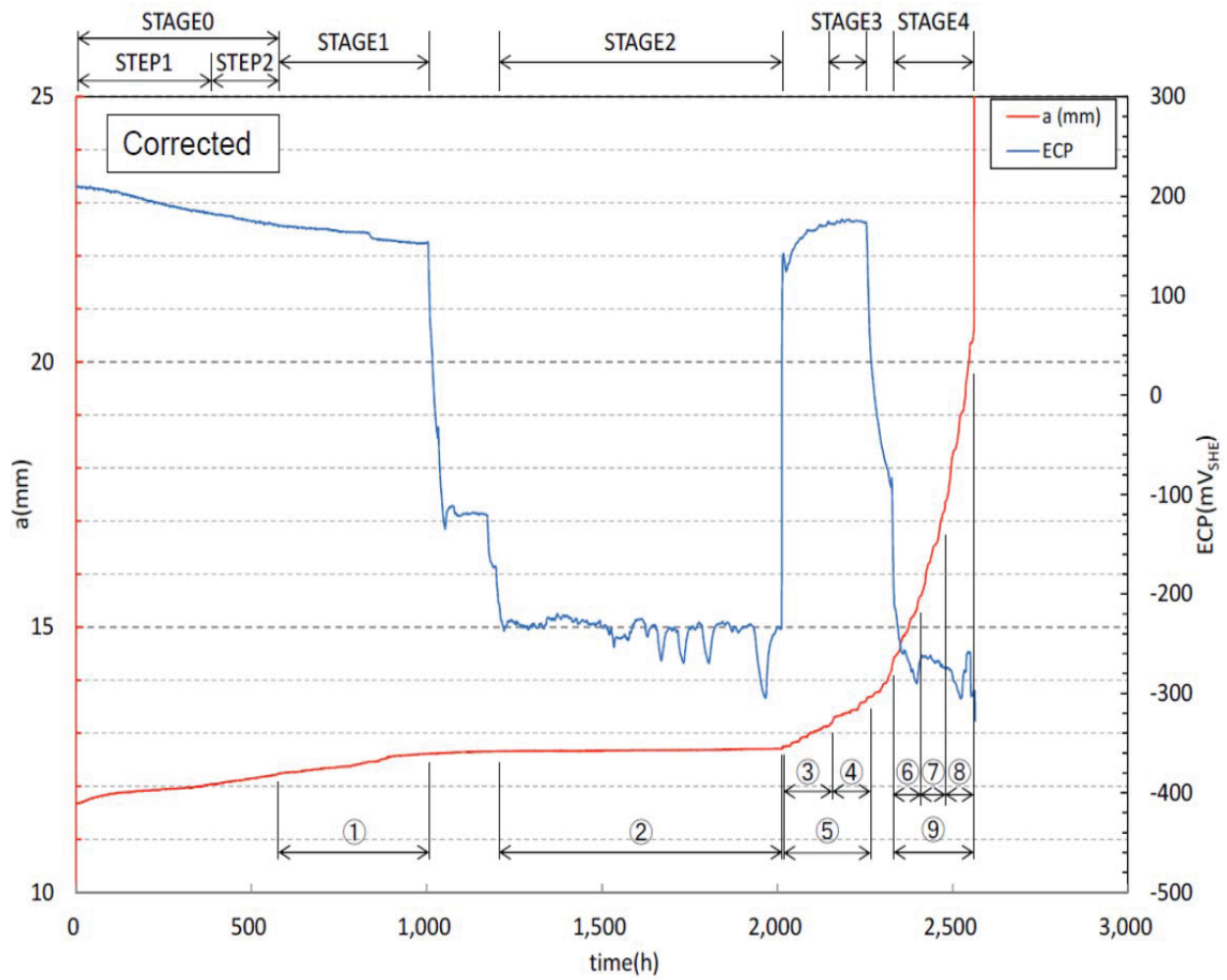


Figure 5. Crack length and corrosion potential versus time during the course of the experiment.

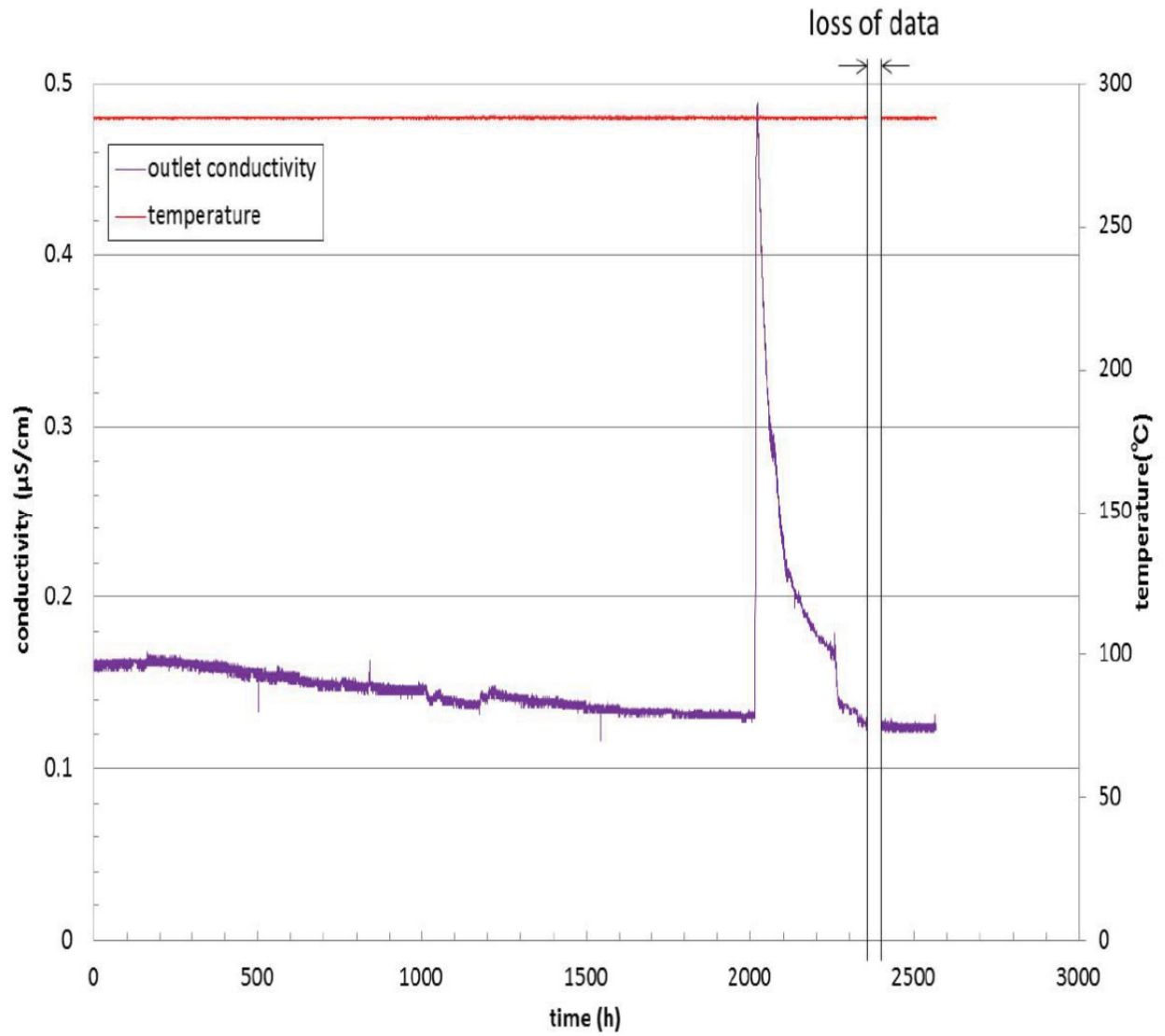


Figure 6. Outlet conductivity and temperature versus time during the course of the experiment.

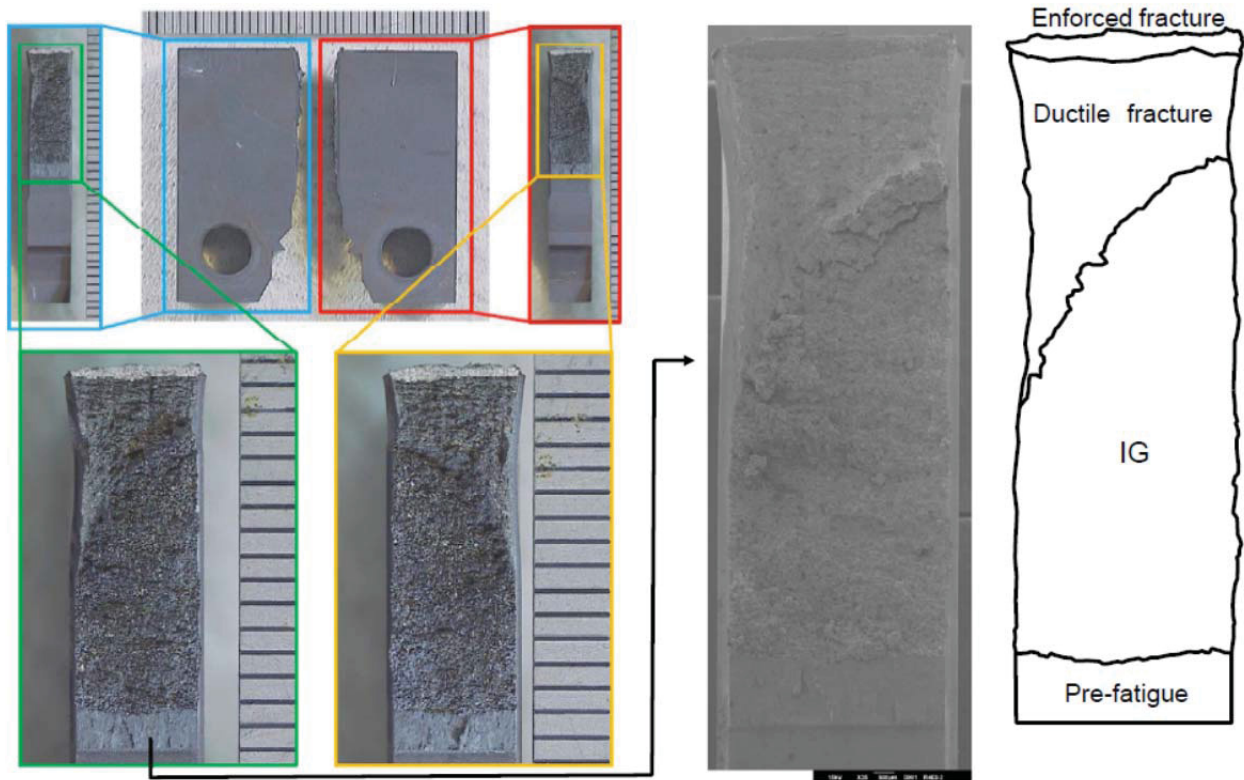


Figure 7. Fracture surface of the CT specimen.

Table 5. CGR obtained for the various test conditions applied.

Region	CGR (m/s)	Average K (MPa $\sqrt{m}$ )	Average ECP (mVshe)	Inlet DO	Inlet DH	Outlet Conductivity ( $\mu\text{S/cm}$ )
(1)	$2.7 \times 10^{-10}$	14.4	162	31.9 ppm	0.3	0.149
(2)	$1.6 \times 10^{-11}$	14.9	-237	5.6 ppb	75.8	0.136
(3)	$9.3 \times 10^{-10}$	15.3	158	32.1 ppm	2.1	0.194 to 0.489
(4)	$1.1 \times 10^{-9}$	16.3	174	30.7 ppm	0.5	0.180
(5)	$1.0 \times 10^{-9}$	15.8	165	31.5 ppm	1.4	0.163 to 0.489
(6)	$4.2 \times 10^{-9}$	20.0	-259	12.9 ppb	78.2	0.128
(7)	$6.6 \times 10^{-9}$	25.4	-268	13.9 ppb	74.2	0.125
(8)	$1.1 \times 10^{-8}$	43.3	-284	10.1 ppb	72.5	0.124
(9)	$7.2 \times 10^{-9}$	29.4	-271	12.1 ppb	73.9	0.125

Stable crack growth behavior was observed in the NWC condition (Stage 1). CGR was  $2.7 \times 10^{-10}$  m/s. After switching to HWC (Stage 2), CGR decreased to  $1.6 \times 10^{-11}$  m/s, demonstrating the mitigation efficiency of HWC. When the environment was switched again to NWC (Stage 3), with an average  $K = 15.3$  MPa $\sqrt{m}$ , CGR increased back to value about four times the value from Stage 1.

After the environment was changed to HWC at Stage 4, there was no decrease of CGR. As crack was propagating and  $K$  was increasing, a rapid increase of CGR was observed. The test was then stopped because the crack opening reached the designated limit of the CGR test equipment. The CGR measured during this experiment is compared with CGR reported in the literature with 304 irradiated in similar

condition in the Japan material testing reactor (Figure 8). CGR measured during Stages 1 through 4 fit well with published data. However, CGR obtained in Regions 6, 7, and 8 are above the data published, which could suggest that we had uncontrolled cracking due to a breach of a K-validity criteria beside the fact that intergranular cracking was observed well after those criteria were breached.

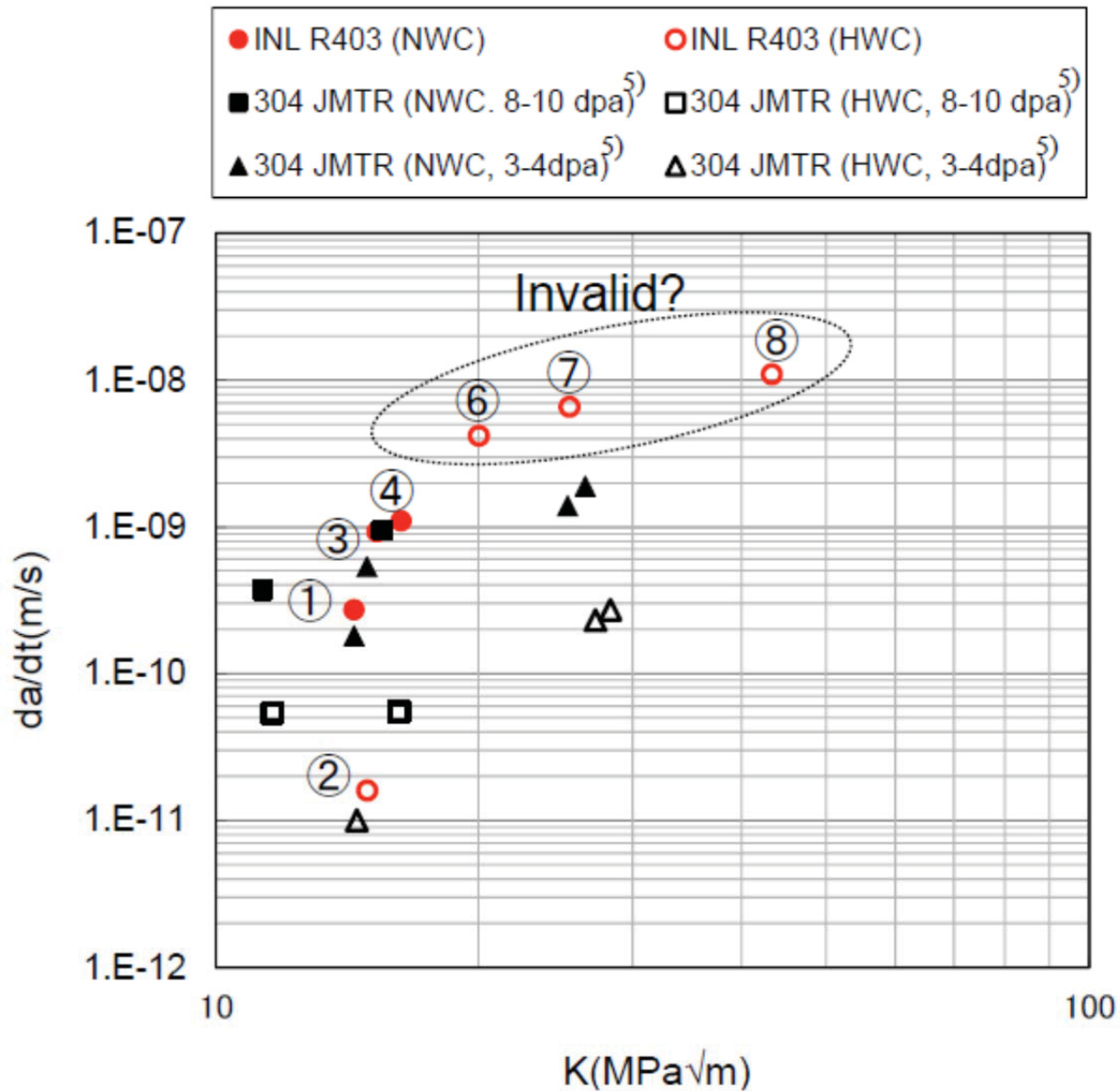


Figure 8. Comparison between the CGR generated during this study and reported data (JNES 2009).

In order to discuss the cause of the rapid fracture, plastic collapse criteria proposed by Kumar (1981, 1984) and the various K-validity criteria were compared with the test results. Figure 9 compares plastic collapse criteria and test results. Arrows indicate the critical load, which satisfied the plastic collapse with plane strain condition or plane stress condition. Rapid fracture seemed to have occurred after the load exceeded the plastic collapse with a plane stress condition. Figure 10 shows a comparison between K-validity criteria for the B dimension and the test results. The K value during the test exceeded the K-validity proposed by Jensen at an early stage. However, there was no sudden change for the trend of crack growth behavior. K value during the test exceeded the K-validity proposed by Andresen just before the rapid fracture. K-validity for B dimension corresponds to the limit for the plane strain condition. After

excess of these criteria, the specimen was thought to be under a plane stress condition. Figure 11 shows a comparison between K-validity criteria for the w-a dimension and test results. The K value during the test exceeded the K-validity after the K value exceeded the plastic collapse with a plane stress condition. Therefore, the K-validity criteria for w-a dimension were not the direct influencing factor on rapid fracture.

Figure 12 shows the relationship between various criteria and the fracture surface. From these considerations, tentative understanding of the observed rapid fracture is thought to be as follows:

- Crack length exceeded K-validity criteria by Andresen for the B dimension and the plane strain condition changed to plane stress condition.
- Load exceeded the plastic collapse criteria (plane stress) and rapid fracture occurred.

However, this hypothesis can be questioned, notably when observing that even the region where plastic collapse occurred showed intergranular fracture. Because only the applied load was constant leading to a rapidly increasing K, it is difficult from this test to differentiate between a rapidly increasing CGR as K increases and an “uncontrolled cracking” because important K-validity criteria were exceeded. The reason for the intergranular fracture is being investigated by sampling material along the crack and characterizing the deformation microstructure.

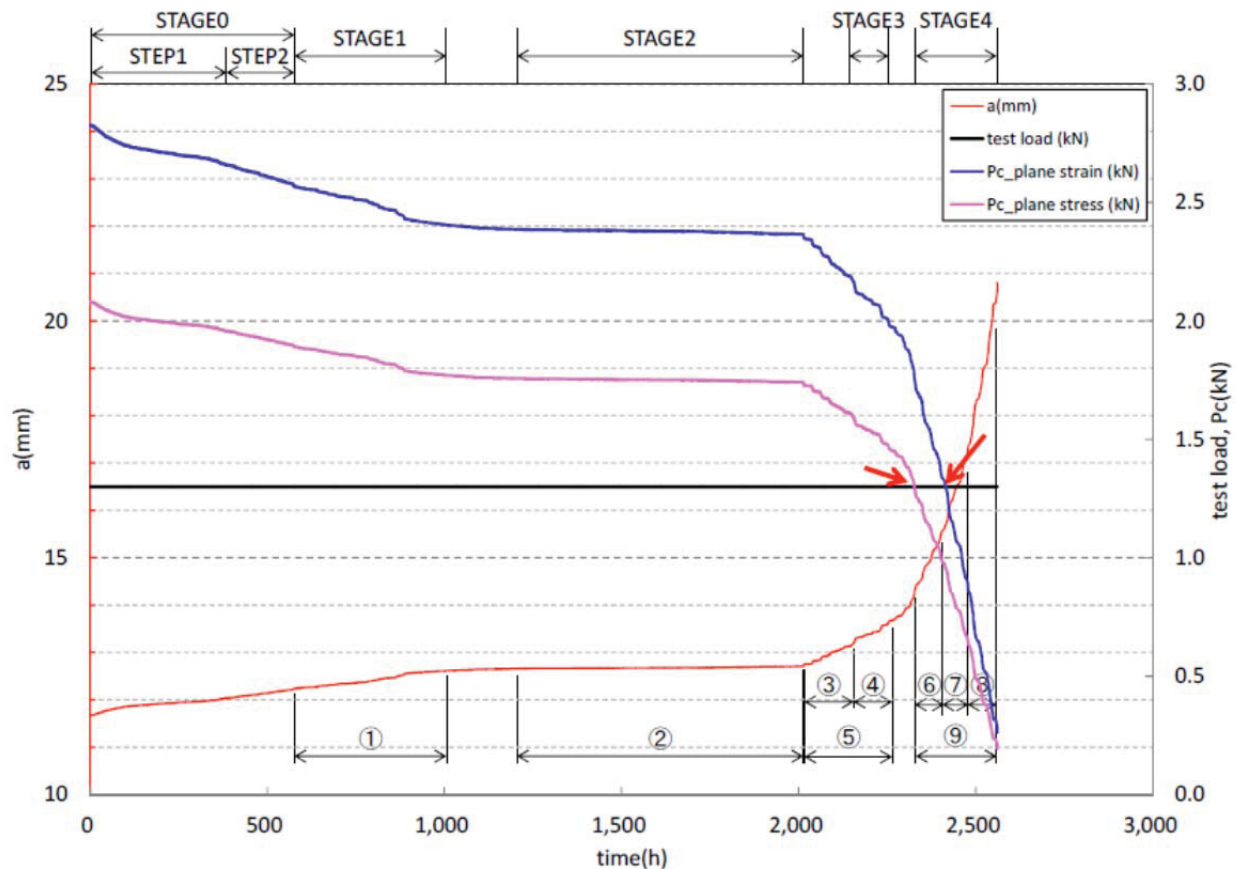


Figure 9. Comparison between plastic collapse criteria and our experimental results.

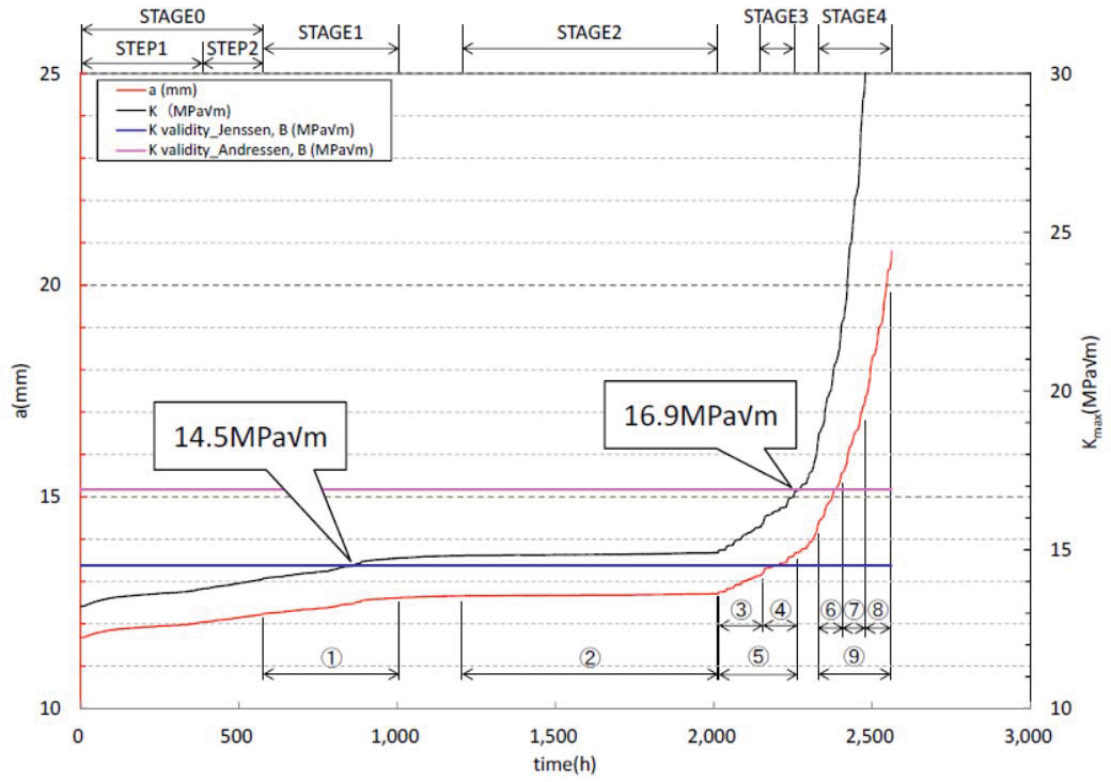


Figure 10. Comparison between K-validity criteria based on B and our experimental results.

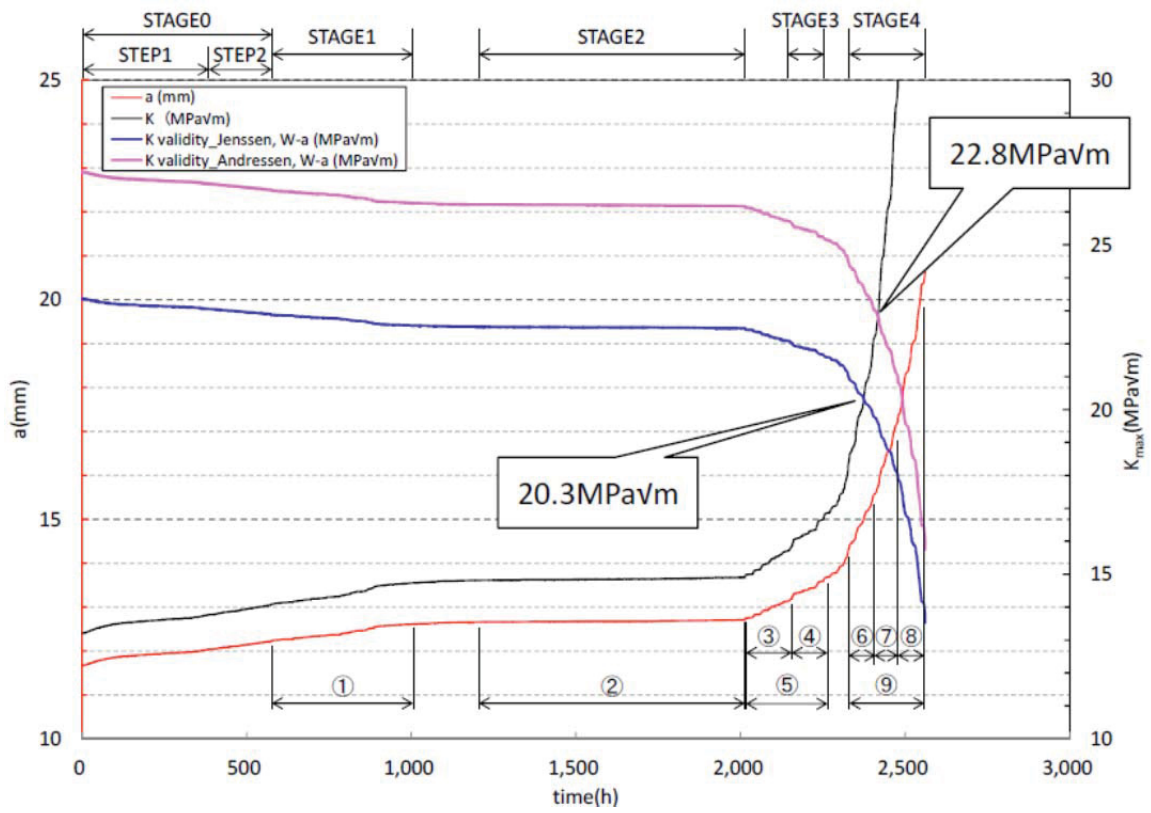


Figure 11. Comparison between K-validity criteria based on (W-a) and experimental results.

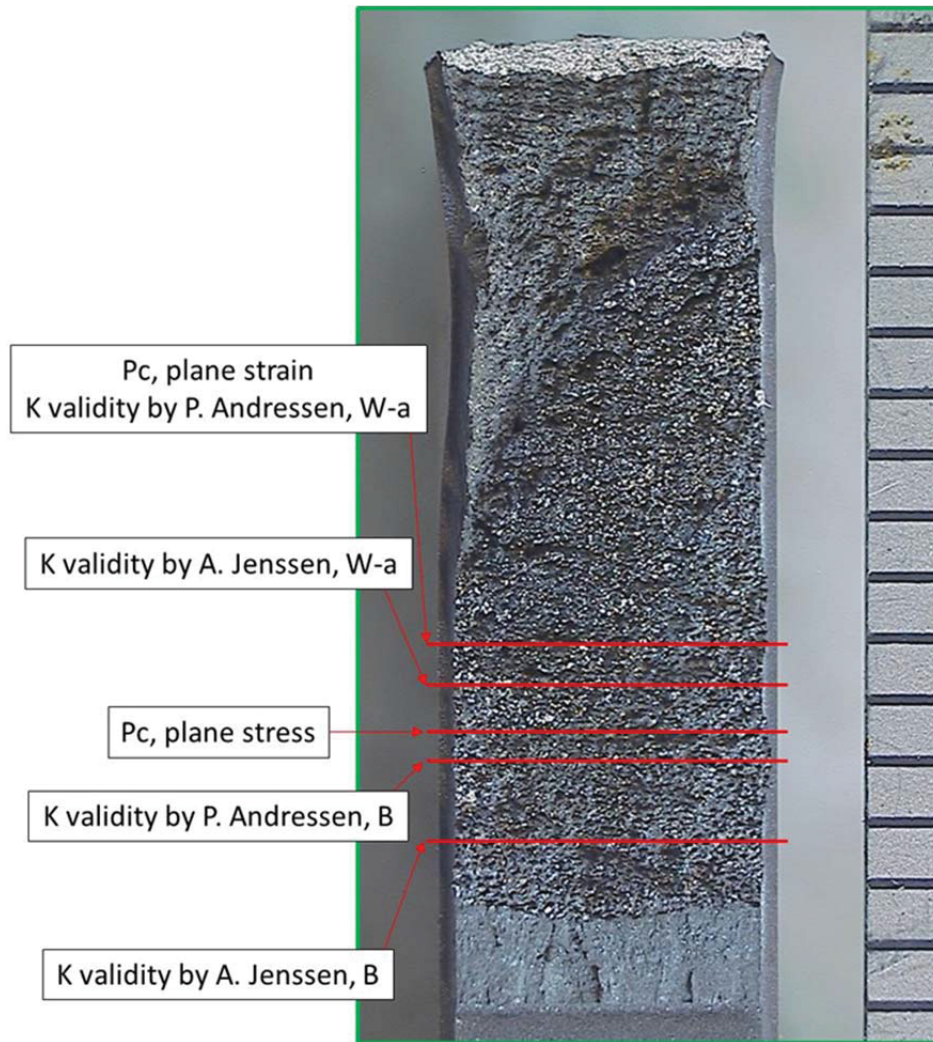


Figure 12. Location of the depth at which the various K-validity criteria were breached on the fracture surface.

#### 4. DEFORMATION MICROSTRUCTURE CHARACTERIZATION PROCEDURE

To investigate the role of deformation on the observed behavior, the deformation microstructure along the crack was observed by sampling the material just under the surface in areas corresponding to the region where the crack grew in conditions that respected all K-size criteria (i.e., Specimen A); a transition region that corresponds to the region where the K-validity criteria based on specimen thickness (B) were breached but not the K-validity criteria based on W-a (Specimen B); and a region where all K-validity criteria, including plastic collapse, were breached (Specimen C). The locations where the specimens were sampled are shown in Figure 13. The transmission electron microscopy foils made using focused ion beam are shown in Figure 14. After sampling, Specimen B probably deformed because of the presence of residual strain in the sample.

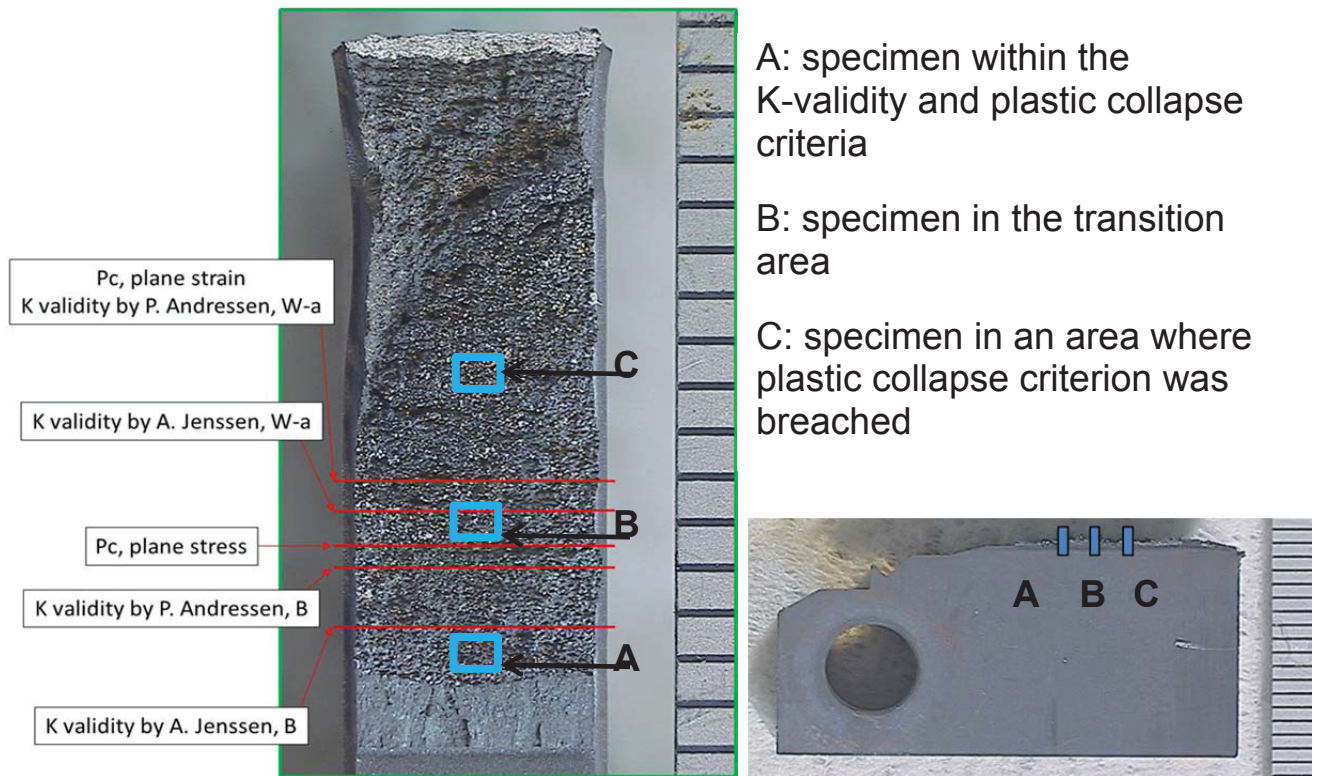


Figure 13. Schematic showing where the test specimens were sampled for analysis of the deformation microstructure.

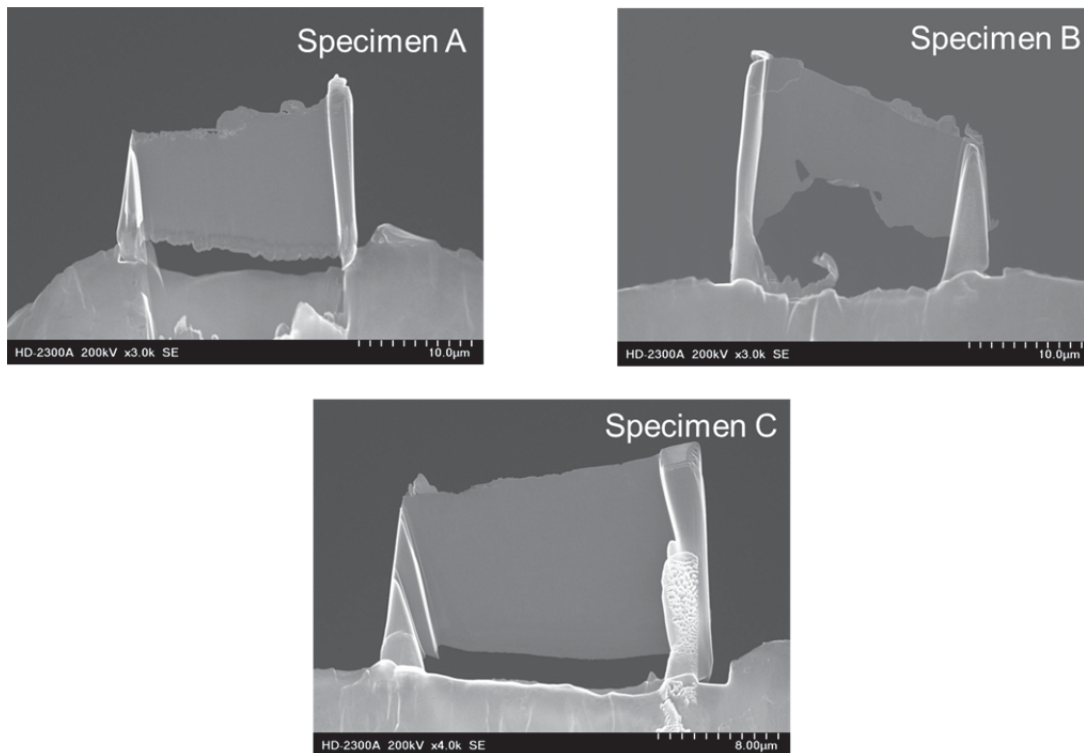


Figure 14. Lift out the transmission electron microscopy specimens for deformation microstructure characterization.

Analysis of the specimens is still ongoing. Initial observation suggests there are no significant differences between the specimen removed in the area where all K-validity criteria were valid (Figure 15) and the one removed in the “transition area.” However, the specimen removed from the area where the plastic collapse criterion was exceeded showed some differences in step-like deformation on a grain boundary and what may be evidence of dislocation channeling (Figure 16). This observation may relate to the intergranular fracture surface observed.

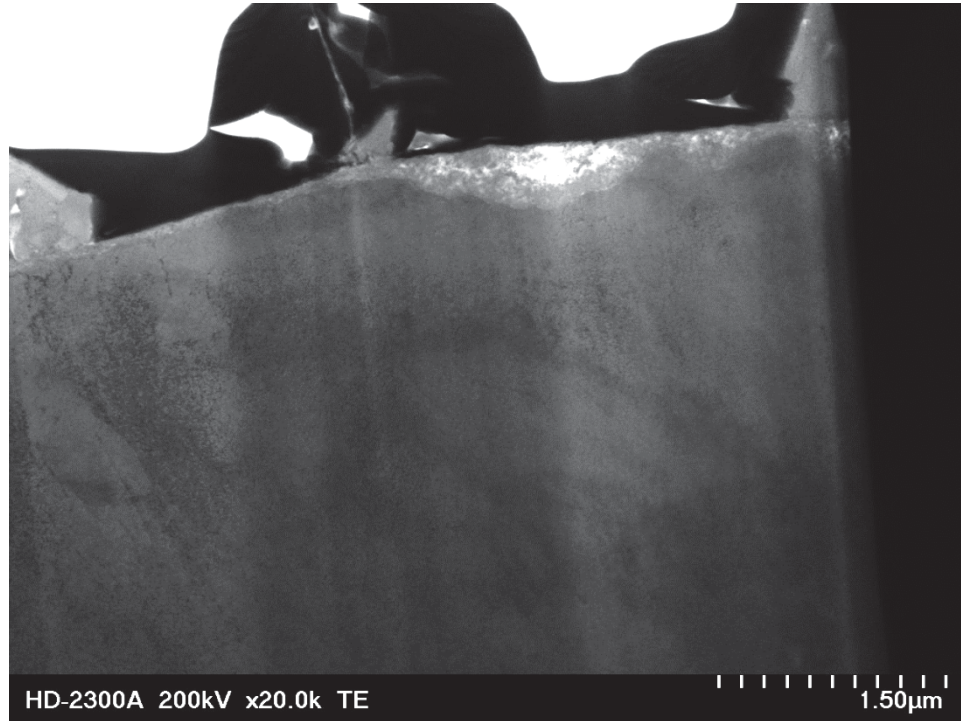


Figure 15. Transmission electron microscopy specimen removed near the IASCC crack in an area corresponding to a crack growing in respect to the K-validity criteria.



Figure 16. Transmission electron microscopy specimen removed near the IASCC crack in an area corresponding to all K-validity criteria that were breached.

## 5. CONCLUSION

The CGR test of a neutron-irradiated Type 304 stainless steel (8.6 dpa) was conducted in simulated BWR conditions. An HWC environment was effective in suppressing the CGR at an early stage of the test (i.e., at lower K). However, HWC was not as effective at later stages of the test and high crack growth was observed during the final stage of the test. The fact that K was not maintained constant (only the load applied was constant) made the end of test hard to control; it is therefore difficult to differentiate between what would be a high CGR in HWC and what is an uncontrolled test because the applied K was too high. It is possible that this behavior is due to the breach of K-validity criteria. However, detailed fracture surface characterization showed that the crack propagated intragranularly well beyond any breach of all K-validity criteria. This leads to questioning the physical signification of the K criteria ,i.e. what changes in the cracking mechanism occur and whether or not the reported loss of HWC efficiency as dose increases for higher applied K would be related to these phenomena.

## 6. REFERENCES

- Andresen, P. L., T. M. Angeliu, L. M. Young, W. R. Catlin, and R. M. Horn, 2002, 10th International Conference on Environmental Degradation of Materials in Nuclear Power Systems– Water Reactors.
- Andresen, P., 2003, “K/Size Effects on SCC in Irradiated, Cold Worked and Unirradiated Stainless Steel,” Proceedings of the Eleventh International Symposium on Environmental Degradation of Materials in Nuclear Power Systems-Water Reactors, American Nuclear Society.
- Andresen, P. L. and M. M. Morra, 2008, *Journal of Nuclear Materials* 383(1-2).
- Hazelton, W. S. and W. H. Koo, 1988, NUREG-0313, Revision 2, U.S. Nuclear Regulatory Commission.
- JAPEIC, 2003, “2003 annual report on the evaluation technology of irradiation assisted stress corrosion cracking (IASCC),” (in Japanese).

- Jensen, A, P. Efsing, K. Gott, and P-O. Andersson, "Crack Growth Behavior of Irradiated Type 304L Stainless Steel in Simulated BWR Environment," Proceedings of the Eleventh International Symposium on Environmental Degradation of Materials in Nuclear Power Systems-Water Reactors, American Nuclear Society.
- Jensen, A., J. Stjarnsater, and R. Pathania, 2009, "Crack Growth Rate Testing of Fast Reactor Irradiated Type 304L and 316 SS in BWR and PWR Environments," 14th International Conference on Environmental Degradation of Materials in Nuclear Power Systems, Virginia Beach, Virginia.
- JNES, 2007, "2007 annual report on the evaluation technology of irradiation assisted stress corrosion cracking (IASCC)" (in Japanese).
- JNES, "2008 annual report on the evaluation technology of irradiation assisted stress corrosion cracking (IASCC)" (2009) (in Japanese).
- Kumar, V., M. D. German, and C. F. Shih, 1981, "An Engineering Approach for Elastic-Plastic Fracture Analysis," EPRI Report NP-1931: 3-3
- Kumar, V. et al., 1984, "Advances in elastic-plastic fracture analysis," final report (Technical Report EPRI-NP-3607), Electric Power Research Institute.
- Nakamura, T., M. Koshiishi, T. Torimaru, Y. Kitsunai, K. Takakura, K. Nakata, M. Ando, Y. Ishiyama, and A. Jensen, 2007, "Correlation between IASCC Growth Behavior and Plastic Zone Size of Crack Tip in 3.5 Neutron Irradiated Type 304L SS CT Specimen," 13th International Conference on Environmental Degradation of Materials in Nuclear Power Systems – Water Reactors, Whistler, British Columbia.
- Takakura, K., K. Nakata, S. Tanaka, T. Nakamura, K. Chatani, and Y. Kaji, 2009, "Crack Growth Behavior of Neutron Irradiated L-Grade Austenitic Stainless Steels in Simulated BWR Conditions," 14th International Conference on Environmental Degradation of Materials in Nuclear Power Systems – Water Reactors, Virginia Beach, Virginia.